

# Dalton Transactions

Accepted Manuscript



This is an *Accepted Manuscript*, which has been through the Royal Society of Chemistry peer review process and has been accepted for publication.

*Accepted Manuscripts* are published online shortly after acceptance, before technical editing, formatting and proof reading. Using this free service, authors can make their results available to the community, in citable form, before we publish the edited article. We will replace this *Accepted Manuscript* with the edited and formatted *Advance Article* as soon as it is available.

You can find more information about *Accepted Manuscripts* in the [Information for Authors](#).

Please note that technical editing may introduce minor changes to the text and/or graphics, which may alter content. The journal's standard [Terms & Conditions](#) and the [Ethical guidelines](#) still apply. In no event shall the Royal Society of Chemistry be held responsible for any errors or omissions in this *Accepted Manuscript* or any consequences arising from the use of any information it contains.

Cite this: DOI: 10.1039/xxxxxxxxxx

## Structural study by solid-state $^{71}\text{Ga}$ NMR of thin film transistor precursors

Blake A. Hammann,<sup>a</sup> Zayd L. Ma,<sup>a</sup> Katherine M. Wentz,<sup>a</sup> Maisha K. Kamunde-Devonish,<sup>b</sup> Darren W. Johnson,<sup>b</sup> and Sophia E. Hayes\*<sup>a</sup>

Received Date

Accepted Date

DOI: 10.1039/xxxxxxxxxx

www.rsc.org/journalname

Solid-state  $^{71}\text{Ga}$  NMR was used to investigate the structures of several heterometallic Group 13 hydroxo-aquo clusters,  $[\text{Ga}_{13-x}\text{In}_x(\mu_3\text{-OH})_6(\mu_2\text{-OH})_{18}(\text{H}_2\text{O})_{24}](\text{NO}_3)_{15}$  which are envisioned for thin film transistors. The characterization of these clusters in the solid state provides additional information in understanding the synthesis, structure and speciation of these precursors for high-quality, ultrasmooth thin films. Yet important structural information regarding these clusters – including the exact composition, isomeric structure, and coordination environments – were unknown prior to this precise NMR spectroscopy study. These molecular species, termed " $\text{Ga}_{13-x}\text{In}_x$ ", contain three types of six-coordinate metal sites, with bridging  $\text{OH}^-$  groups and  $\text{H}_2\text{O}$  as capping ligands, and we report results on  $\text{Ga}_7\text{In}_6$ ,  $\text{Ga}_8\text{In}_5$ ,  $\text{Ga}_{10}\text{In}_3$ ,  $\text{Ga}_{11}\text{In}_2$ ,  $\text{Ga}_{12}\text{In}_1$ , and  $\text{Ga}_{13}$ . Utilizing two magnetic fields (13.9 T and 21.1 T), the solid-state NMR spectra were interpreted in conjunction with computational modeling (using CASTEP) and simulation of spectral lineshapes (using Dmfit). The metal sites are best represented as distorted octahedra, and they exhibit a range of quadrupolar couplings and asymmetry parameters, which can be addressed using longitudinal strain analysis. Until now, there has been speculation about the sites for transmetallation within the synthetic cluster community. Here, we show that Ga NMR is a powerful technique to monitor the transmetallation of In for Ga in the  $\text{Ga}_{13-x}\text{In}_x$  clusters, specifically substituting in the "outer ring" sites, and not the "core" or "middle ring."

## 1 Introduction

High quality metal-oxide semiconductors have emerged as a key component in the production of next-generation thin film devices. Metal-oxide films can be prepared by a variety of methods, but recently, solution processing routes have become viable due to the scalability of depositing large area films.<sup>2-4</sup> Indium-gallium-oxide (IGO) films are just one material of interest because they can be prepared from aqueous solution precursors and deposited via spin-coating techniques.<sup>1,4,5</sup>

Aqueous heterometallic nanoscale tridecameric cluster precursors such as  $[\text{Ga}_{13-x}\text{In}_x(\mu_3\text{-OH})_6(\mu_2\text{-OH})_{18}(\text{H}_2\text{O})_{24}]^{15+}$  ( $x = 1$  to 6) have gained attention in the material science community because of their ability to form high density metal-oxide films<sup>1,5-7</sup>.

The semiconductor industry has seen an increasing use of gallium and indium as key components for III/V semiconductors along with other  $p$ -block amorphous metal oxide semiconductors.<sup>8</sup> The resulting films from the cluster precursors are envisioned as dense, high-quality metal oxide dielectrics.<sup>1,6,7</sup> The complexes are capable of being prepared from solution-based methods on the gram scale and deposited onto substrates via solution condensation processes such as spin coating and spray coating.<sup>1,5-7</sup> With industry moving towards more environmentally and economically friendly procedures, the water-based heterometallic hydroxo-aquo complexes have the potential to become a new route for high quality thin films.

Recently, these heterometallic molecular complexes have been characterized using solution-state  $^1\text{H}$  nuclear magnetic resonance (NMR) spectroscopy and by single crystal X-ray diffraction (XRD).<sup>9,10</sup> Single crystal structures of the two cluster end products,  $[\text{Ga}_{13}(\mu_3\text{-OH})_6(\mu_2\text{-OH})_{18}(\text{H}_2\text{O})_{24}]^{15+}$  and  $[\text{Ga}_7\text{In}_6(\mu_3\text{-OH})_6(\mu_2\text{-OH})_{18}(\text{H}_2\text{O})_{24}]^{15+}$ , have been previously published,<sup>1,11</sup> and the corresponding heterometallic species were more recently characterized by a combination of single crystal and powder XRD.<sup>10</sup> While single crystal XRD is a useful tool, it is difficult to fully characterize the clusters based solely on this method be-

<sup>a</sup> Department of Chemistry, Washington University in St. Louis, St. Louis, MO, 63130-4899, USA. Fax: +1-314-935-4481; Tel: +1-314-935-4624; E-mail: hayes@wustl.edu

<sup>b</sup> Department of Chemistry and Biochemistry, University of Oregon, Eugene, OR, 97403-1253, USA.

† Electronic Supplementary Information (ESI) available: Notes on CASTEP calculations, Magnetic field comparison between 21.1 T and 13.9T of the mixed metal hydroxo-aquo clusters,  $^{71}\text{Ga}$  3QMAS NMR of the  $\text{Ga}_7\text{In}_6$  cluster, Table of Ideal bond lengths for the clusters, and a Table of the Dmfit simulation parameters. See DOI: 10.1039/b000000x/

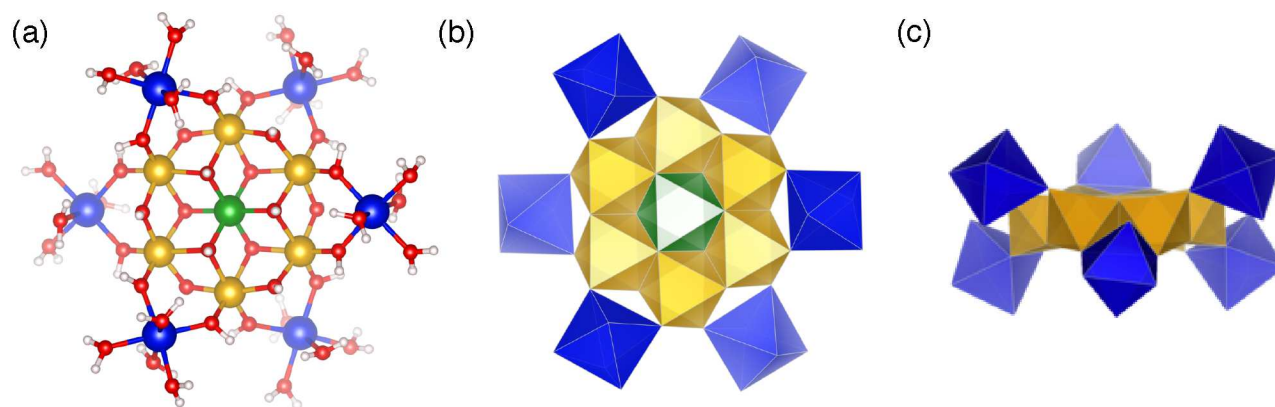


**Fig. 1** Representations of a **Ga<sub>7</sub>In<sub>6</sub>** structure,  $[\text{Ga}_7\text{In}_6(\mu_3\text{-OH})_6(\mu_2\text{-OH})_{18}(\text{H}_2\text{O})_{24}]^{15+}$ . Metal sites are colored green, amber, and blue; O and H are shown as red and white, respectively. (a) Atoms are located according to prior single crystal XRD results of **Ga<sub>7</sub>In<sub>6</sub>**<sup>1</sup>. Space-filling polyhedra (octahedra) show: (b) overhead polyhedral view of the **Ga<sub>7</sub>In<sub>6</sub>** cluster and (c) a polyhedral side view of the **Ga<sub>7</sub>In<sub>6</sub>** cluster. The polyhedra show the “core” (green), “middle ring” (amber), and “outer ring” (blue) metal sites with hydrogens and oxygens omitted for clarity. The structure contains additional 15  $\text{NO}_3^-$  species (not shown) to charge balance the cluster.

cause it is unable to resolve any amorphous domains, impurities, and disorder in either the counterions or the substituted metal ions that are present. A complementary tool such as solid-state NMR (ssNMR) provides a means to elucidate the structure and assess the purity of the cluster samples for the first time. NMR is a unique characterization tool for these metal-oxide clusters because quadrupolar nuclei that comprise the six-coordinate metal centers are sensitive to the local environment (e.g., bond angles, bond lengths, and the proximity of counterions) allowing characterization of the coordination environment, isomeric composition, and bulk disorder in these dynamic clusters.

We present a <sup>71</sup>Ga NMR characterization study through experimental measurements and modeling of several tridecameric gallium-indium heterometallic clusters with the formula of  $[\text{Ga}_{13-x}\text{In}_x(\mu_3\text{-OH})_6(\mu_2\text{-OH})_{18}(\text{H}_2\text{O})_{24}]^{15+}$  (hereafter referred to as “**Ga<sub>13-x</sub>In<sub>x</sub>**”). The clusters studied here are **Ga<sub>7</sub>In<sub>6</sub>**, **Ga<sub>8</sub>In<sub>5</sub>**, **Ga<sub>10</sub>In<sub>3</sub>**, **Ga<sub>11</sub>In<sub>2</sub>**, and **Ga<sub>12</sub>In<sub>1</sub>**. The structure of **Ga<sub>13</sub>** has been studied by ssNMR spectroscopy previously,<sup>12</sup> and we depict it here as a guide to the gallium sites that are present. These heterometallic clusters share a common motif (Figure 1): a planar group of six-coordinate gallium sites which consists of one gallium atom at the center (“core”) connected via  $\mu_3$ -OH bridges to a “middle ring” of six gallium atoms. The middle ring of gallium atoms is connected to the outer metal sites (“outer ring”), which are also six-coordinate, by  $\mu_2$ -OH bridges (Figure 1a). The outer ring consists of six remaining metal sites where gallium may be replaced by indium through transmetallation reactions.<sup>5,10</sup> Single crystal XRD and, as we will show, ssNMR of the **Ga<sub>7</sub>In<sub>6</sub>** both show that the indium atoms replace only the outer gallium sites as they are incorporated into the cluster.<sup>1</sup>

Combining NMR at high magnetic fields with fast magic-angle-spinning (MAS), enables the characterization of these heterometallic clusters thus permitting determination of the quadrupolar lineshapes that results from perturbations introduced by the indium-substituted sites.

## 2 Experimental

### 2.1 Synthesis

The synthesis and characterization of all clusters have been reported elsewhere.<sup>1,10</sup>  $\text{Ga}(\text{NO}_3)_3$  and  $\text{In}(\text{NO}_3)_3$  salt hydrates were dissolved in methanol, and di-butyl nitrosoamine (DBNA) was added to this solution. The solution was stirred, uncapped, and then left undisturbed in air at room temperature. Within two weeks, most of the solvent evaporated, leaving colorless, block-shaped single crystals which were isolated from the bottom of the vials by removing the DBNA and washing with acetone. The reagent ratios for the clusters may be found in the literature.<sup>10,11</sup> The composition of each of the clusters has been established by elemental analysis along with single crystal XRD which yields the average standard deviation for the composition.<sup>10</sup>

### 2.2 Solid-State NMR

<sup>71</sup>Ga solid-state NMR data were acquired at two magnetic field strengths 13.9 T and 21.1 T corresponding to <sup>71</sup>Ga Larmor frequencies of 179.89 MHz and 274.42 MHz, respectively. All spectra were obtained using a quadrupolar-echo<sup>13</sup> pulse sequence ( $\pi/2 - \tau - \pi$ ) under rotor-synchronized magic angle spinning (MAS) conditions of  $\nu_R = 33$  kHz (at 13.9 T) and  $\nu_R = 62.5$  kHz (at 21.1 T). All pulses used were central transition selective. The recycle delays were 200 ms at both magnetic fields. All spectra were referenced at 0 ppm to a 1.0 M solution of  $\text{Ga}(\text{NO}_3)_3$  dissolved in water. The 13.9 T data were acquired using a Tecmag Redstone spectrometer equipped with a Bruker 2.5 mm HX MAS probe. 21.1 T data were acquired using a Bruker Avance II console equipped with a Bruker 1.3 mm HX MAS probe. <sup>71</sup>Ga 3QMAS NMR spectrum was recorded for the **Ga<sub>7</sub>In<sub>6</sub>** cluster (see Supplementary Information†) on a 2.5 mm HX MAS Bruker probe at 21.1 T.

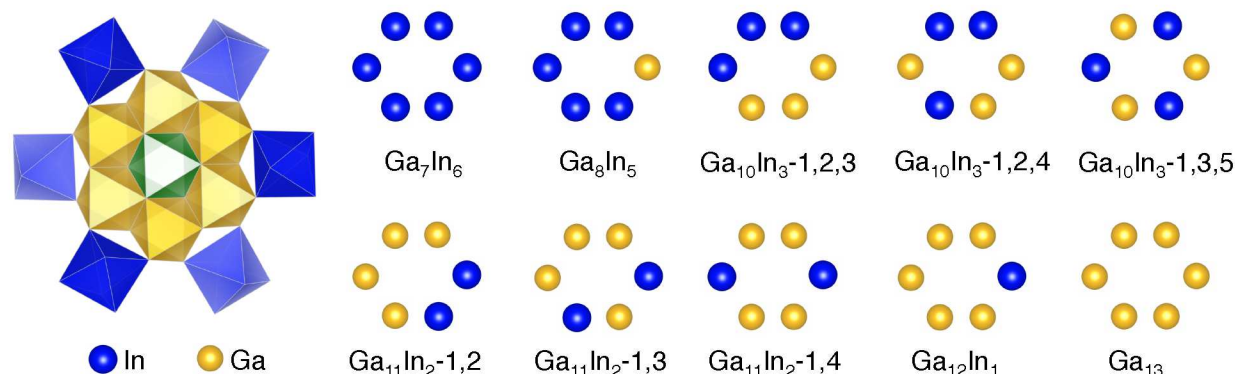


**Fig. 2** Polyhedral representation of the tridecameric cluster. Assuming substitution of outer sites only, the possible isomers for the various In-substituted species are represented by the amber and blue circles, depicting In in blue and Ga in amber.

### 2.3 NMR Spectral Fitting

The experimental spectra were simulated using Dmfit<sup>14</sup> using previously-determined parameters determined for the related  $\text{Ga}_{13}$  cluster<sup>12</sup> to provide initial guesses for fitting. The 21.1 T dataset of the  $\text{Ga}_7\text{In}_6$  cluster were fit first assuming the presence of two types of gallium sites and using the “core” and “middle ring” parameters from the  $\text{Ga}_{13}$  cluster as starting points. The intensity, isotropic chemical shift ( $\delta_{iso}$ ), asymmetry ( $\eta_Q$ ), and quadrupole coupling ( $C_Q$ ) were allowed to “float” in the program. The fitting process was continued in an iterative manner, allowing Dmfit to adjust the parameters until the program converged onto a model lineshape of the experimental NMR data. The best fit parameters were then iterated between the two magnetic fields to converge the NMR model lineshape. Supplementary information Table S2<sup>†</sup> contains all parameters required for the fits.

### 2.4 Longitudinal and Shear Strain Analysis

Longitudinal strain and shear strain analysis<sup>15</sup> was performed on the individual clusters using inputs for bond lengths and bond angles from the single crystal XRD data. Longitudinal strain,  $|\alpha|$ , refers to the deviation of the M-O ( $M = \text{Ga}, \text{In}$ ) bond length from an ideal polyhedron bond. Longitudinal strain is calculated by  $|\alpha| = \sum |\ln(I_i/I_o)|$ , where  $I_i$  and  $I_o$  are the actual and ideal M-O bond lengths, respectively.<sup>15</sup> This ideal bond length is calculated based on the volume of the polyhedron. The shear strain ( $|\psi|$ ) represents deviation of the O-M-O bond angles from an ideal polyhedron, and it is calculated by  $|\psi| = \sum |\tan(\theta_i/\theta_o)|$ , where  $\theta_i$  and  $\theta_o$  are the actual and ideal O-M-O bond angles, respectively.<sup>15</sup>

### 2.5 Computational Methods

Materials Studio CASTEP version 7.0<sup>16</sup> was used to perform density functional theory (DFT) calculations of NMR parameters using crystallographic data as inputs. DFT<sup>17,18</sup> calculations used the generalized gradient approximations (GGA) and the Perdew-Burke-Ernzerhof (PBE) functionals.<sup>19–21</sup> Computation of shielding tensors and electric field gradient<sup>22</sup> tensors were performed using the GIPAW<sup>23,24</sup> method. Ultrasoft-pseudo potentials<sup>24</sup> were used and calculated “on-the-fly” within the Materials Studio Client, and a precise plane-wave cutoff energy of 610 eV was

specified. Optimization of all atomic positions were conducted with a  $3 \times 5 \times 2$  Monkhorst-Pack k-point grid.

The heterometallic clusters crystallize in a hexagonal crystal lattice with a space group of  $R\bar{3}$ . The unit cells have a volume of  $\sim 6500 \text{ \AA}^3$  for  $\text{Ga}_{13}$  and  $\sim 6800 \text{ \AA}^3$  for  $\text{Ga}_7\text{In}_6$ . In order to calculate a system this large and complicated, a significant amount of computational time is required. Therefore, the calculations resorted to stripping the unit cell down to the bare cluster with nitrate counterions to charge balance it. It is worthy to note that the computational data inputs (such as atomic coordinates) were first generated using the SQUEEZE<sup>25</sup> version of the single-crystal XRD data sets. Such post-processed X-ray diffraction data are not an accurate representation of the precise local structure; here, the fractional occupancy of some nitrate counterions is not accounted for, nor are the exact positions of the In sites due to positional disorder. In order to achieve a better computational fit to the experimental data, the pre-SQUEEZE processed XRD data were needed to probe the local environment surrounding the individual gallium sites, by including  $\text{NO}_3^-$  groups into the CASTEP calculations.

For the  $\text{Ga}_{13}$  and  $\text{Ga}_7\text{In}_6$  clusters, calculations were performed with fifteen nitrate counterions in order to closely model the electrostatic potential surrounding the clusters. In addition, Figure 2 shows schematically the various isomers that can be present for all the  $\text{Ga}_{13-x}\text{In}_x$  clusters. These isomers, along with the lack of long-range order in how the molecules are arranged in the crystal (positional disorder) leads to highly complex crystal structures for  $\text{Ga}_8\text{In}_5$  thru  $\text{Ga}_{12}\text{In}_1$ .  $\text{Ga}_8\text{In}_5$ ,  $\text{Ga}_{10}\text{In}_3$ ,  $\text{Ga}_{11}\text{In}_2$ , and  $\text{Ga}_{12}\text{In}_1$  could not be modeled owing to the lack of long-range order that would require very large “super cells” to adequately capture their structure variability. Geometry optimization was performed on the clusters which allowed all atomic positions to relax and resulted in the best computational fit to the experimental quadrupolar parameters. The calculated  $\delta_{iso}$ ,  $C_Q$ , and  $\eta_Q$  (Table 1) are average values for the middle and outer ring sites. The calculated  $\delta_{iso}$  was calculated by  $\delta_{iso} = \sigma_{iso} - \sigma_{ref}$ , where  $\sigma_{iso}$  is the isotropic shielding and  $\sigma_{ref} = 1502$  ppm was used from reference Middlemiss *et al.*<sup>26</sup>.

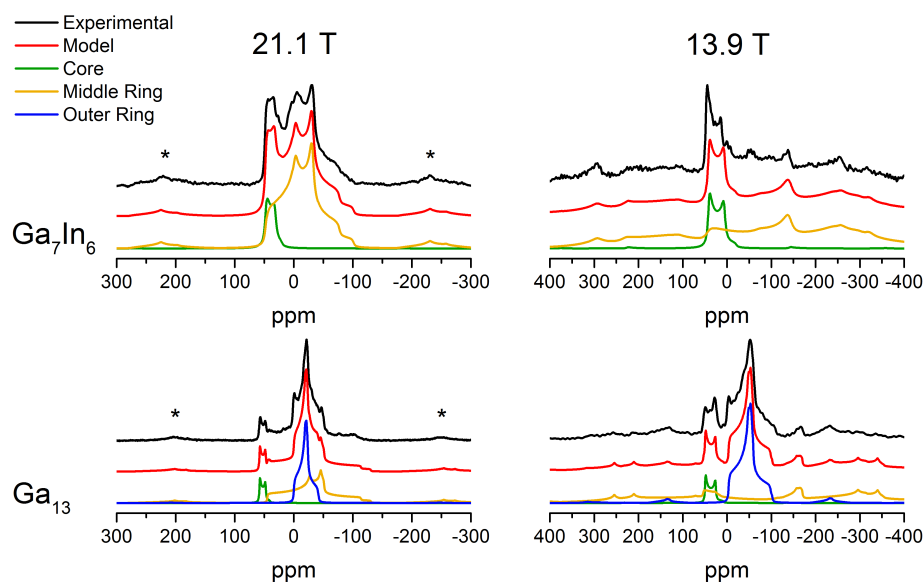


**Fig. 3**  $^{71}\text{Ga}$  MAS NMR of the  $\text{Ga}_7\text{In}_6$  and  $\text{Ga}_{13}$  clusters at two magnetic field strengths 21.1 T (left column) and 13.9 T (right column) and spinning at 62.5 kHz (21.1 T) and 33 kHz (13.9 T). Each plot is broken down into 3 traces: black (top) is experimental data, red (middle) is the Dmfit model composed of lineshapes in green “core,” amber “middle ring,” and blue “outer ring” (bottom). \* denote spinning sidebands.

### 3 Results and Discussion

Gallium has two NMR-active isotopes,  $^{69}\text{Ga}$  and  $^{71}\text{Ga}$ , with natural abundances of approximately 60% and 40%, respectively. Both nuclei are quadrupolar with a nuclear spin of  $I = 3/2$ , and consequently the interactions of the electric field gradient (EFG) with the nuclear quadrupole moment ( $eQ$ ) need to be considered.<sup>27</sup> This quadrupole coupling causes broadening of the NMR resonance, and when second order quadrupole broadening dominates, the shape of the NMR resonance can be described by the quadrupolar coupling constant  $C_Q = e^2qQ/h$  and asymmetry parameter  $\eta_Q = (V_{xx} - V_{yy})/V_{zz}$ .<sup>28</sup> Where  $eQ$  is the nuclear quadrupolar moment,  $eq$  is the principal field gradient (defined as  $eq = V_{zz}$ ),  $h$  is Planck’s constant, and  $V_{xx}$ ,  $V_{yy}$ , and  $V_{zz}$  are the elements of the diagonalized tensor for the electric field gradient, whose elements can be determined by singularities in the NMR lineshape. Under rapid magic angle spinning (MAS), interactions from chemical shift anisotropy, direct dipole-dipole coupling, and first-order quadrupole interactions are averaged to zero; however, second-order quadrupole interactions with the EFG are not completely averaged to zero and still need to be taken into account.<sup>28</sup> Although  $^{71}\text{Ga}$  has a lower natural abundance than  $^{69}\text{Ga}$ , it has a smaller quadrupole moment than  $^{69}\text{Ga}$  resulting in higher sensitivity due to narrower NMR resonances, thus making it the preferred nucleus for study.

We recently reported the  $^{69}\text{Ga}$  and  $^{71}\text{Ga}$  solid-state NMR characterization of  $\text{Ga}_{13}$ <sup>12</sup> (reproduced in the bottom spectrum of Figure 3), distinguishing three types of six-coordinate gallium sites and correlating their quadrupolar lineshapes with distortions of the local environment. We reproduce the spectrum here because  $\text{Ga}_{13}$  serves as a guide for the NMR characterization of the corresponding sites in the  $\text{Ga}_{13-x}\text{In}_x$  heterometallic clusters.

The  $^{71}\text{Ga}$  MAS NMR spectrum of the  $\text{Ga}_7\text{In}_6$  heterometallic

cluster is shown in Figure 3 along with a deconvolution of the experimental spectrum at 21.1 T and 13.9 T. The NMR data show that the resonances comprise only the core (green) and middle (amber) Ga species; the outer sites as seen in  $\text{Ga}_{13}$  (in blue) are absent in the  $\text{Ga}_7\text{In}_6$ . The chemical shifts for the observed NMR resonances confirmed the identities of six-coordinate Ga in the heterometallic clusters, which is consistent with the single-crystal XRD. Six-coordinate gallium is normally found in the chemical shift range of -50 to +50 ppm, while four-coordinate gallium in found in the range of +100 to +200 ppm. In order to verify the EFG model parameters, NMR spectra were acquired at two magnetic field strengths, 13.9 T and 21.1 T. In the Supplementary Information, Table S2†, the parameters ( $\delta_{iso}$ ,  $C_Q$ , and  $\eta_Q$ ) used to generate the lineshapes in Dmfit for  $\text{Ga}_{13}$  and  $\text{Ga}_7\text{In}_6$  at both magnetic fields are provided. The additional indium in the outer ring results in slight changes to  $\eta_Q$ , since gallium will experience a distribution of neighbors in its coordination sphere.

#### 3.1 CASTEP

A computational study for two of the highly ordered heterometallic clusters,  $\text{Ga}_{13}$  and  $\text{Ga}_7\text{In}_6$ , was undertaken to investigate the local environment of the gallium atoms. With the recent developments in first-principles calculations (the Gauge Including Projector Augmented Waves [GIPAW]),<sup>23</sup> the accurate calculation of NMR parameters has been significantly advanced. The application of Density Functional Theory (DFT) to the calculation of NMR parameters has been demonstrated in a number of chemical systems,<sup>29</sup> and it has been recently demonstrated on heavy atoms in metal-oxide systems.<sup>26</sup> Here we possess single-crystal XRD structures of  $\text{Ga}_{13}$  and  $\text{Ga}_7\text{In}_6$ , which yield coordinates for each of the atoms. Consequently, these inputs allow us to model the NMR quadrupolar parameters for the most or-

dered species,  $\text{Ga}_7\text{In}_6$  and  $\text{Ga}_{13}$  (i.e., those without isomers or positional disorder to complicate the analysis). The ability to calculate NMR parameters that closely match the experimental data results in a unique complementary tool for spectral assignments (details for the calculations can be found in the Supplementary Information†).

The calculated quadrupolar parameters are listed in Table 1 for the  $\text{Ga}_{13}$  and  $\text{Ga}_7\text{In}_6$  structures, and these are in close agreement with the experimental data, following similar trends. In both  $\text{Ga}_{13}$  and  $\text{Ga}_7\text{In}_6$ , the core site remains in an environment of high symmetry with asymmetry parameters ( $\eta_Q$ ) that are close to zero. The calculated core  $C_Q$  increases with the incorporation of indium, which is also reflected in the experimental data. The quadrupolar coupling is the smallest for the core site, followed by the outer ring, and then the middle ring. This trend follows the symmetry of the six coordinate Ga species going from a high symmetry  $C_{3v}$  site at the core to the outer ring Ga with (nearly)  $C_{2v}$  symmetry, to the low symmetry middle ring Ga (with  $C_1$  symmetry). The asymmetry is the largest in the outer ring (the Ga site that possess four  $\text{H}_2\text{O}$  ligands and the two  $\mu_2\text{-OH}$  bonds), followed by the middle ring (with its mixture of  $\mu\text{-OH}$  bonds), and then the core (with six  $\mu_3\text{-OH}$  bonds). While the computational evidence is not exact for the middle ring, the best evidence that the calculations have closely modeled the environments of the gallium metal sites is the observed trends in the  $C_Q$  and  $\eta_Q$  from the  $\text{Ga}_{13}$  to the  $\text{Ga}_7\text{In}_6$  cluster.

### 3.2 NMR results

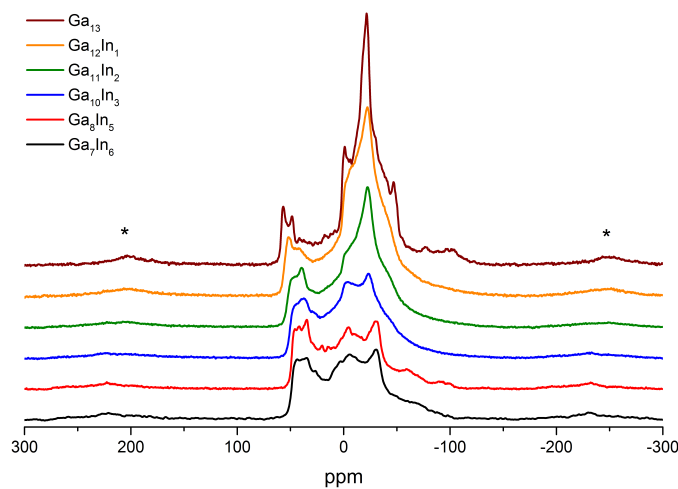


**Fig. 4**  $^{71}\text{Ga}$  MAS NMR of the  $\text{Ga}_7\text{In}_6$ ,  $\text{Ga}_8\text{In}_5$ ,  $\text{Ga}_{10}\text{In}_3$ ,  $\text{Ga}_{11}\text{In}_2$ ,  $\text{Ga}_{12}\text{In}_1$ , and  $\text{Ga}_{13}$  clusters at 21.1 T and spinning at 62.5 kHz (21.1 T). \* denote spinning sidebands.

In Figure 4, we show the  $^{71}\text{Ga}$  MAS NMR spectra for a series of heterometallic  $\text{Ga}_{13-x}\text{In}_x$  clusters.  $\text{Ga}_{12}\text{In}_1$ ,  $\text{Ga}_{11}\text{In}_2$ , and  $\text{Ga}_{10}\text{In}_3$  all show evidence of disorder arising from the combination of the different isomers that may be present due to positional disorder (random orientation of the In substituted sites on the outer ring), and the fractional occupancy of the nitrate counterions in the lat-

tice. These three types of perturbations to the long-range structure lead to broadening and smoothing of the NMR lineshapes. Deconvolutions of such lineshapes are possible but less exact than in the ordered end members,  $\text{Ga}_{13}$  and  $\text{Ga}_7\text{In}_6$ . The  $\text{Ga}_8\text{In}_5$  spectrum is nearly identical to that of the  $\text{Ga}_7\text{In}_6$ , with no obvious broadening or smoothing of the resonances (addressed below).

Using the lineshapes of Figure 3 as a guide, these spectra have been deconvoluted to yield parameters of  $C_Q$ ,  $\eta_Q$ , and  $\delta_{iso}$  given in Table 2. (Supplementary information Figure S1† shows the experimental data and deconvolutions at two field strengths for this series of spectra.)

The most striking feature is that the core Ga site is always apparent as a narrower lineshape on the high-frequency side of the spectra. As seen in Table 2, the  $C_Q$  changes, as a result of the indium incorporation, by over 20% from 5.0 MHz (for  $\text{Ga}_{13}$ ) to 6.1 MHz ( $\text{Ga}_7\text{In}_6$ ) indicating that the core site has experienced larger distortions. Since the core site is narrow and clearly resolved, it is the most readily modeled with  $\eta_Q$  and  $C_Q$  values. In addition to 1D MAS spectra, a  $^{71}\text{Ga}$  3QMAS NMR spectrum was acquired on the  $\text{Ga}_7\text{In}_6$  cluster (see Supplementary Information Figure S2†). Due to the efficiency of the MQMAS experiment being dependent on  $C_Q$ ,<sup>30,31</sup> the only site observed was that of the core  $C_Q \sim 6$  MHz, and 3QMAS is consistent with the 1D MAS data.

The outer Ga sites are well defined for  $\text{Ga}_{13}$ ,  $\text{Ga}_{12}\text{In}_1$ , and  $\text{Ga}_{11}\text{In}_2$  and as expected, absent for  $\text{Ga}_7\text{In}_6$  (consistent with XRD data). The outer ring is discernible for the  $\text{Ga}_{10}\text{In}_3$ , but overlaps strongly with the rest of the NMR pattern. The outer Ga sites are all fairly similar, with the most discernible trend being an increase in  $C_Q$  with In incorporation. The  $\text{Ga}_8\text{In}_5$  spectrum is nearly identical to that of  $\text{Ga}_7\text{In}_6$  with no obvious intensity from an outer ring gallium in the  $\text{Ga}_8\text{In}_5$ . One would expect a resonance of approximately equal integrated intensity to that of the core in  $\text{Ga}_8\text{In}_5$  spectrum, and we hypothesize that the lone outer gallium is broadened too much to be visible in the NMR data because there is no crystallographic ordering of that single gallium. Therefore, its positional disorder may cause this Ga site to be in a different secondary coordination environments.

The middle sites are the most difficult to resolve spectroscopically, because they have the largest  $C_Q$  at  $\sim 13$  MHz. The  $\text{Ga}_7\text{In}_6$  cluster has a well-defined lineshape at the higher magnetic field (21.1 T), which allows for effective extraction of the quadrupolar parameters. The middle ring gallium site is barely evident at 13.9 T, and it is too broad to be well resolved, except via line fitting at 21.1 T. The addition of In species in  $\text{Ga}_7\text{In}_6$  does not alter the middle ring Ga resonance appreciably; the  $C_Q$  values are comparable to that of  $\text{Ga}_{13}$ . However,  $\eta_Q$  becomes more symmetric with In incorporation as a combination of changes to Ga-O bond lengths and O-Ga-O bond angles. Notably, the 3QMAS NMR spectrum could not be used to resolve the middle sites.

### 3.3 Longitudinal Strain

Longitudinal and shear strain analyses can help establish the relationship between quadrupolar parameters such as  $\eta_Q$  and  $C_Q$  and the distortion of octahedral sites. As demonstrated by Ghose and Tsang<sup>32</sup>, deviation of bond lengths and angles from an ideal six-

**Table 1**  $^{71}\text{Ga}$  NMR experimental data computed using CASTEP for the  $\text{Ga}_7\text{In}_6$  and  $\text{Ga}_{13}$  clusters. Geometry optimized structures for the heterometallic clusters were calculated within the CASTEP code taking average  $\delta_{iso}$ ,  $C_Q$ , and  $\eta_Q$  for the middle and outer ring gallium atoms.

Cluster	$C_Q$ (MHz)			$\eta_Q$			$\delta_{iso}$ (ppm)		
	Core	Middle	Outer	Core	Middle	Outer	Core	Middle	Outer
$\text{Ga}_7\text{In}_6$ (Exp.) <sup>a</sup>	6.12	13.11	-	0.05	0.62	-	51.20	50.56	-
$\text{Ga}_7\text{In}_6$ (Comp.) <sup>b</sup>	6.22	12.85	-	0.03	0.74	-	41.35	75.36	-
$\text{Ga}_{13}$ (Exp.) <sup>a,c</sup>	5.00	13.91	6.72	0.00	0.78	0.90	60.73	45.58	-0.62
$\text{Ga}_{13}$ (Comp.) <sup>b</sup>	5.88	12.2	9.38	0.00	0.49	0.95	60.78	48.6	93.57

a) "Exp." are the parameters used to simulate the experimental lineshapes shown in Figure 3 ( $^{71}\text{Ga}$  NMR).

b) "Comp." are the values from CASTEP computations on geometry optimized clusters including fifteen  $\text{NO}_3^-$  anions to charge balance it.

c) Parameters are reproduced from reference Ma *et al.* <sup>12</sup>.

**Table 2**  $^{71}\text{Ga}$  NMR experimental parameters at 21.1 T from Dmfit used for the simulation of NMR lineshapes for the various  $\text{Ga}_{13-x}\text{In}_x$  clusters at 21.1 T in Figure 4 ( $^{71}\text{Ga}$  NMR).

Cluster	$C_Q$ (MHz)			$\eta_Q$			$\delta_{iso}$ (ppm)		
	Core	Middle	Outer	Core	Middle	Outer	Core	Middle	Outer
$\text{Ga}_7\text{In}_6$	6.1	13.1	-	0.05	0.62	-	51	51	-
$\text{Ga}_8\text{In}_5$	6.1	12.9	-	0.09	0.61	-	52	48	-
$\text{Ga}_{10}\text{In}_3$	5.9	13.1	7.6	0.02	0.58	0.84	52.8	50.1	5
$\text{Ga}_{11}\text{In}_2$	5.9	13.4	7.3	0.01	0.50	0.9	55.3	52.7	2
$\text{Ga}_{12}\text{In}_1$	5.8	14.0	7.5	0.01	0.63	0.84	58	58	3
$\text{Ga}_{13}$ <sup>a</sup>	5.0	13.9	6.7	0.00	0.78	0.90	61	46	-1

a) Parameters are reproduced from reference Ma *et al.* <sup>12</sup>.

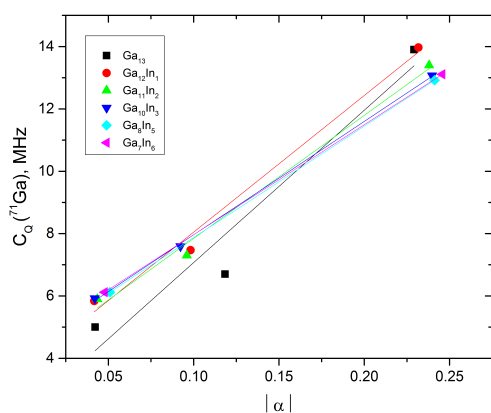


**Fig. 5** The  $^{71}\text{Ga}$  quadrupolar coupling constant ( $C_Q$ ) as a function of the longitudinal strain ( $|\alpha|$ ) (the deviation of the M-O bond ( $M = \text{Ga}, \text{In}$ ) lengths from ideal).

coordinate octahedron can be reflected in two parameters, longitudinal strain and shear strain.

Longitudinal strain ( $|\alpha|$ ) describes the distortions to the M-O bond lengths, where M is the metal (Ga or In) and O is oxygen, that deviates from the bond length for an ideal octahedron with the same volume. Similarly, shear strain  $|\psi|$  describes the deviation of the O-M-O bond angle from an ideal octahedral bond angle of  $90^\circ$ . Using the atomic coordinates from the single crystal XRD data, we are able to calculate the longitudinal and shear strain from the analysis of the bond lengths and angles. (At times average distances, meaning In-O and Ga-O, and bond angles must be used since In has a fractional occupancy of the outer ring sites.)

The six-coordinate sites present in the tridecameric clusters offer an opportunity to correlate longitudinal strain with the mea-

sured quadrupolar coupling constant,  $C_Q$ . (Notably, there is no correlation between  $C_Q$  and  $|\psi|$ , the shear strain parameter for six-coordinate Al-O species<sup>15</sup>). Table 3 lists the values calculated for  $|\alpha|$ , for core, middle ring, and outer ring sites, for the series of clusters studied here. Figure 5 shows a plot of  $C_Q$  versus  $|\alpha|$ , with the identity of each cluster indicated in the legend. There is a linear correlation between the calculated value of  $|\alpha|$  as a measure of Ga-O bond length distortions and the experimental measurement of  $C_Q$ . Our results are in agreement with trends found in  $^{27}\text{Al}$  NMR of aluminosilicates, where a correlation to six-coordinate Al was found for  $|\alpha|$  but none for  $|\psi|$ .<sup>32</sup>

The trend in  $C_Q$  also matches the symmetry properties of the different sites. The core site is axially symmetric as a trigonal antiprism, possessing a three-fold axis ( $C_{3v}$  in Schönflies notation), and has the lowest  $C_Q$ . The outer sites have nearly  $C_{2v}$  symmetry and fall in the middle of the correlation plot. The largest  $C_Q$  values are found for the lowest-symmetry ( $C_1$ ) middle ring sites, and they also have the largest values for  $|\alpha|$  in the series.

**Table 3** Longitudinal strain analyses of the heterometallic Group 13 clusters in this study. Both the middle and outer values are calculations that are based on the average M-O bond lengths ( $M = \text{Ga}, \text{In}$ ), since the XRD has fractional occupancy of gallium or indium in the outer sites. Octahedron volume for the individual metal sites and the ideal bond lengths are presented in Supplementary Information Table S1†. The percent change (% Change) was calculated for the difference between  $\text{Ga}_{13}$  and  $\text{Ga}_7\text{In}_6$ .

Cluster	Core $ \alpha $	Middle Ring $ \alpha $	Outer Ring $ \alpha $
$\text{Ga}_7\text{In}_6$	0.0478	0.246	-
$\text{Ga}_8\text{In}_5$	0.0509	0.242	-
$\text{Ga}_{10}\text{In}_3$	0.0420	0.240	0.0923
$\text{Ga}_{11}\text{In}_2$	0.0435	0.238	0.0960
$\text{Ga}_{12}\text{In}_1$	0.0417	0.232	0.098
$\text{Ga}_{13}$	0.0423	0.229	0.118
% Change	+12%	+6.9%	

Looking at the datasets as a whole and referring to Figure 4 and Supplementary Information Figure S1†, several key points emerge. The middle ring sites are consistently the broadest in linewidth ( $C_Q$  at  $\sim 13$  MHz), significantly larger than that of the other two sites. As such, their fitting is always complicated by having the spectrum spread over such a large range. The outer ring site has a similar appearance for the  $\text{Ga}_{13}$  and  $\text{Ga}_{12}\text{In}_1$  species. The similarity of the outer ring resonance for  $\text{Ga}_{13}$  and  $\text{Ga}_{12}\text{In}_1$  is suggestive that the perturbations from a neighboring indium are minimal, indicating little structural distortions to the outer octahedra. This finding of little structural distortion is reinforced by the longitudinal strain analysis for the outer ring sites. The neighboring In species for  $\text{Ga}_7\text{In}_6$  appear to have minimal influence on the middle ring  $C_Q$  values while causing broadening with the core site, a trend that is reflected in  $|\alpha|$ , as well.

## 4 Conclusions

A series of heterometallic clusters were studied by  $^{71}\text{Ga}$  solid-state NMR, deconvoluting complex lineshapes into three types of six-coordinate Ga sites: core, middle ring, and outer ring. The crystalline species,  $\text{Ga}_7\text{In}_6$  and  $\text{Ga}_{13}$  were used in conjunction with CASTEP first-principles calculations to extract quadrupolar parameters for the lineshapes. These were then extended as "initial guesses" to simulate spectra using Dmfit for the less-ordered species,  $\text{Ga}_8\text{In}_5$ ,  $\text{Ga}_{10}\text{In}_3$ ,  $\text{Ga}_{11}\text{In}_2$ ,  $\text{Ga}_{12}\text{In}_1$ , which all exhibit a combination of positional disorder and potentially multiple isomers (for  $\text{Ga}_{10}\text{In}_3$  and  $\text{Ga}_{11}\text{In}_2$ ).

The  $^{71}\text{Ga}$  MAS NMR results confirm that indium substitution only occurs at outer ring positions. There are trends in  $C_Q$  and  $\eta_Q$  which are discernible, and longitudinal strain analysis — correlating perturbations to bond lengths in six-coordinate sites with the quadrupolar coupling parameter — shows a linear correlation between  $C_Q$  and  $|\alpha|$  for the different types of sites (their correspondingly distorted "octahedra").

The core site is well-resolved and trends related to it can be easily discriminated: with increasing In content,  $C_Q$  increases, largely from changes in bond length, while  $\eta_Q$  remains fairly steady in this series.

The outer ring site is obtained through line fitting, and its values change only slightly as In is incorporated, as these sites are not directly connected to the locations of In substitution. Given that the coordination environment for the outer ring Ga sites consists of four  $\text{H}_2\text{O}$  ligands and two  $\mu\text{-OH}$  ligands, the electric field gradient is dominated by these different substituents more than other perturbative influences from the In.

The middle ring sites are, therefore, elucidated only through CASTEP calculations and Dmfit lineshape simulations. The  $C_Q$  values are largest of the three sites, and addition of In does not lead to a distinguishable trend with respect to  $C_Q$ . However,  $\eta_Q$  values do become smaller with In substitution, suggesting that the six  $\mu\text{-OH}$  bonds surrounding the middle ring shift with In incorporation to create less distortion to the middle ring site than that found in the  $\text{Ga}_{13}$  parent species.

Gaining insight into the distortions of local chemical environments in these clusters and the effect of these on the NMR quadrupolar lineshapes is important for analyzing the thin films

eventually produced from these precursors.

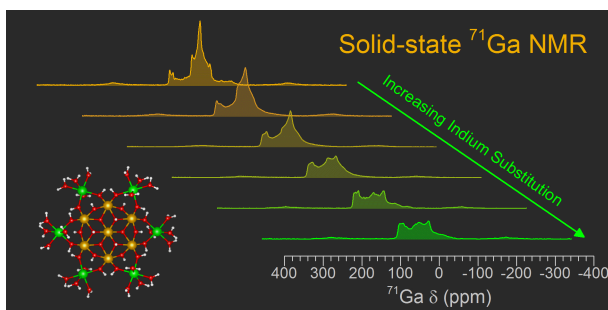
## 5 Acknowledgements

This material is based on work in the Center for Sustainable Materials Chemistry, which is supported by the National Science Foundation under Grant CHE-1102637. Victor V. Terskikh is thanked for acquiring the 21.1 T NMR spectra at the National Ultrahigh-Field NMR Facility for Solids (Ottawa, Canada), a national research facility funded by the Canada Foundation for Innovation, the Ontario Innovation Trust, Recherche Quebec, and Bruker Biospin and managed by the University of Ottawa (<http://nmr900.ca>). Computations were performed using the Washington University Center for High Performance Computing (CHPC), partially supported through grant NCR1S10RR022984-01A1. Malcolm Tobias is thanked for computational support on the CHPC cluster.

## References

- 1 Z. Mensinger, J. Gatlin, S. Meyers, L. Zakharov, D. Keszler and D. Johnson, *Angewandte Chemie International Edition*, 2008, **47**, 9484–9486.
- 2 S. J. Kim, S. Yoon and H. J. Kim, *Japanese Journal of Applied Physics*, 2014, **53**, 02BA02.
- 3 S. R. Thomas, P. Pattanasattayavong and T. D. Anthopoulos, *Chem. Soc. Rev.*, 2013, **42**, 6910–6923.
- 4 A. Nadarajah, M. Z. B. Wu, K. Archila, M. G. Kast, A. M. Smith, T. H. Chiang, D. A. Keszler, J. F. Wager and S. W. Boettcher, *Chemistry of Materials*, 2015.
- 5 M. K. Kamunde-Devonish, M. N. Jackson, Z. L. Mensinger, L. N. Zakharov and D. W. Johnson, *Inorganic Chemistry*, 2014, **53**, 7101–7105.
- 6 J. Anderson, C. Munsee, C. Hung, T. Phung, G. Herman, D. Johnson, J. Wager and D. Keszler, *Advanced Functional Materials*, 2007, **17**, 2117–2124.
- 7 S. T. Meyers, J. T. Anderson, D. Hong, C. M. Hung, J. F. Wager and D. A. Keszler, *Chemistry of Materials*, 2007, **19**, 4023–4029.
- 8 Z. L. Mensinger, W. Wang, D. A. Keszler and D. W. Johnson, *Chem. Soc. Rev.*, 2012, **41**, 1019–1030.
- 9 A. Oliveri, L. A. Wills, C. R. Hazlett, M. E. Carnes, I.-Y. Chang, P. Cheong and D. Johnson, *Chem. Sci.*, 2015, **6**, 4071–4085.
- 10 M. K. Kamunde-Devonish, D. B. Fast, Z. L. Mensinger, J. T. Gatlin, L. N. Zakharov, M. R. Dolgos and D. W. Johnson, *Inorganic Chemistry*, 2015, **54**, 3913–3920.
- 11 E. Rather, J. T. Gatlin, P. G. Nixon, T. Tsukamoto, V. Kravtsov and D. W. Johnson, *Journal of the American Chemical Society*, 2005, **127**, 3242–3243.
- 12 Z. L. Ma, K. M. Wentz, B. A. Hammann, I.-Y. Chang, M. K. Kamunde-Devonish, P. H.-Y. Cheong, D. W. Johnson, V. V. Terskikh and S. E. Hayes, *Chemistry of Materials*, 2014, **26**, 4978–4983.
- 13 F. H. Larsen, H. J. Jakobsen, P. D. Ellis and N. C. Nielsen, *Journal of Magnetic Resonance*, 1998, **131**, 144 – 147.
- 14 D. Massiot, F. Fayon, M. Capron, I. King, S. Le Calvé, B. Alonso, J.-O. Durand, B. Bujoli, Z. Gan and G. Hoatson,

- Magnetic Resonance in Chemistry*, 2002, **40**, 70–76.
- 15 K. J. D. MacKenzie and M. E. Smith, *Multinuclear Solid-State NMR of Inorganic Materials*, Elsevier Science Ltd, 2002.
- 16 S. J. Clark, M. D. Segall, C. J. Pickard, P. J. Hasnip, M. I. J. Probert, K. Refson and M. C. Payne, *Zeitschrift für Kristallographie*, 2005, **220**, 567–570.
- 17 P. Hohenberg and W. Kohn, *Phys. Rev.*, 1964, **136**, B864–B871.
- 18 W. Kohn and L. J. Sham, *Phys. Rev.*, 1965, **140**, A1133–A1138.
- 19 J. P. Perdew, K. Burke and M. Ernzerhof, *Phys. Rev. Lett.*, 1996, **77**, 3865–3868.
- 20 J. P. Perdew, K. Burke and M. Ernzerhof, *Phys. Rev. Lett.*, 1998, **80**, 891–891.
- 21 B. Hammer, L. B. Hansen and J. K. Nørskov, *Phys. Rev. B*, 1999, **59**, 7413–7421.
- 22 M. Profeta, C. Pickard and F. Mauri, *J. Am. Chem. Soc.*, 2003, **125**, 2541–548.
- 23 C. Pickard and F. Mauri, *Phys. Rev. B*, 2001, **63**, 245101.
- 24 J. Yates, C. Pickard and F. Mauri, *Phys. Rev. B*, 2007, **76**, 024401.
- 25 P. van der Sluis and A. L. Spek, *Acta Crystallographica Section A*, 1990, **46**, 194–201.
- 26 D. S. Middlemiss, F. Blanc, C. J. Pickard and C. P. Grey, *Journal of Magnetic Resonance*, 2010, **204**, 1 – 10.
- 27 P. Man, *Encyclopedia of Magnetic Resonance*, J. Wiley, 2007.
- 28 *NMR of Quadrupolar Nuclei in Solid Materials*, ed. R. E. Wasylshen, S. E. Ashbrook and S. Wimperis, Wiley, 2012.
- 29 C. Bonhomme, C. Gervais, F. Babonneau, C. Coelho, F. Pourpoint, T. Azas, S. E. Ashbrook, J. M. Griffin, J. R. Yates, F. Mauri and et al., *Chem. Rev.*, 2012, **112**, 5733–5779.
- 30 G. Wu, D. Rovnyak and R. G. Griffin, *Journal of the American Chemical Society*, 1996, **118**, 9326–9332.
- 31 D. Massiot, T. Vosegaard, N. Magneron, D. Trumeau, V. Montouillout, P. Berthet, T. Loiseau and B. Bujoli, *Solid State Nuclear Magnetic Resonance*, 1999, **15**, 159 – 169.
- 32 S. Ghose and T. Tsang, *American Mineralogist*, 1973, **58**, 748–755.



$^{71}\text{Ga}$  NMR yields lineshapes that reflect the different coordination environments in tridecameric “ $\text{Ga}_{13-x}\text{In}_x$ ” hydroxo-aquo clusters,  $[\text{Ga}_{13-x}\text{In}_x(\mu_3\text{-OH})_6(\mu_2\text{-OH})_{18}(\text{H}_2\text{O})_{24}]$ . Indium substitution is found only in the peripheral “outer” metal sites (shown in green).